PCCP

Accepted Manuscript

ROYAL SOCIETY OF CHEMISTRY

www.rsc.org/pccp

Journal Name

RSCPublishing

COMMUNICATION

Competition between electron transfer, trapping, and recombination in CdS nanorod-hydrogenase complexes†

Cite this: DOI: 10.1039/xoxxoooooox

James K. Utterback,[a] Molly B. Wilker,[a] Katherine A. Brown,[b] Paul W. King,[b] Joel D. Eaves,[a] and Gordana Dukovic*[a]

Received ooth January 2012,
Accepted ooth January 2012

DOI: 10.1039/xoxxoooooox

www.rsc.org/

Electron transfer from photoexcited CdS nanorods to [FeFe]-hydrogenase is a critical step in photochemical H_2 production by CdS-hydrogenase complexes. By accounting for the distributions in the numbers of electron traps and enzymes adsorbed, we determine rate constants and quantum efficiencies for electron transfer from transient absorption measurements.

Coupling semiconductor nanocrystals to redox enzymes is an emerging strategy to photochemically drive fuel-generating reactions such as H_2 production and CO_2 reduction.[1-9] These hybrid structures integrate the tunable electronic structure, strong light absorption, and surface chemistry of nanocrystals with the catalytic selectivity of enzymes. Photochemical reactions of nanocrystal-enzyme complexes proceed through a sequence of steps: light absorption in the nanocrystals, transfer of photoexcited electrons to the enzyme where they participate in catalysis, and hole scavenging by sacrificial electron donors.[2, 5, 7] The kinetics of electron transfer (ET) from the nanocrystal to the enzyme play a crucial role in the overall photochemical reactivity. The quantum efficiency of ET (QE_{ET}) determines the upper limit on the quantum yield of fuel generation. QE_{ET}, in turn, depends on how the rate of ET compares to the rates of competing excited state decay processes in the nanocrystal, such as radiative and nonradiative recombination and carrier trapping. We have recently measured electron decay kinetics in complexes of CdS nanorods (NRs) with [FeFe]-hydrogenase I from *Clostridium acetobutylicum* (CaI), which photochemically reduces $2H^+$ to H_2.[2] Transient absorption (TA) spectra recorded over a time window of 10^{-13}–10^{-4} s indicate that ET occurs on a similar timescale as the excited state decay of NRs.[2] Similar results were reported in complexes of CdTe quantum dots and CaI.[4]

Quantifying the interplay between ET and the competing relaxation processes is critical for increasing the photochemical efficiency of nanocrystal-enzyme hybrids. Understanding the kinetics of nanocrystal-enzyme ET is complicated by the fact the excited states of nanocrystals decay nonexponentially over many decades in time, even in the absence of catalysts.[10, 11, 12] These dynamics reflect the structural heterogeneities present in nanocrystal samples, some of which arise from variations in the number of carrier trapping sites on the nanocrystal surface.[11, 13] Adsorption of enzymes further increases sample heterogeneity.[1] Average electron lifetimes in CdS NR and CdS–CaI ensemble samples can be determined from multiexponential and/or stretched exponential fits to TA data.[2] However, these lifetimes do not provide the intrinsic rate constants for the excited state decay processes because they do not take into account the underlying sample heterogeneity, i.e., the number distribution of electron traps and enzymes per NR in the ensemble. Thus, to understand how electron decay processes in CdS NRs compete with ET to CaI, it is necessary to use a kinetic model that accounts for population heterogeneities.

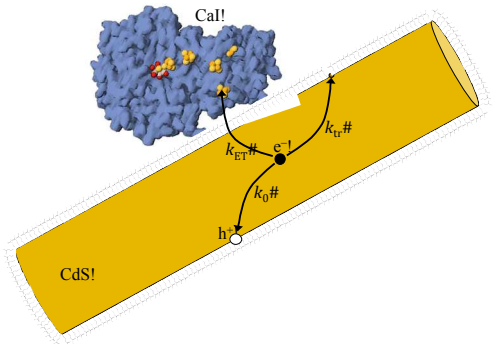

Scheme 1 Schematic depiction of photoexcited electron decay pathways in a CdS–CaI complex, including electron-hole recombination (k_0), electron trapping (k_{tr}) and electron transfer (k_{ET}).

In this communication, we employ such a model to analyze the decay of the electron population observed in the TA signal of CdS NRs and CdS–CaI complexes in the 1–100 ns time window. We determine the intrinsic rate constants, i.e. probabilities per unit time that a particular microscopic relaxation event occurs, for three electron decay processes: electron-hole recombination in CdS NRs (k_0), electron trapping (k_{tr}), and ET to CaI (k_{ET}) (Scheme 1). In this model, the numbers of the electron trap sites and adsorbed CaI moieties follow independent Poisson distributions. We find k_0 to be 1.5×10^7 s^{-1}, and k_{tr} to be 7-fold larger (1.1×10^8 s^{-1}), with the

average electron trap density ($\langle N_{tr} \rangle$) of 0.59 per NR. From a series of CdS–CaI samples with varying CdS:CaI molar ratios, we find that k_{ET} (2.4×10^7 s^{-1}) is within a factor of two of k_0. QE_{ET} in the ensemble sample is a function of both the ratios of the intrinsic rate constants and of the average numbers of traps and enzymes. While it depends strongly on the ratio k_{ET}/k_0, the dependence on k_{tr}/k_0 is weak because $\langle N_{tr} \rangle$ is small, causing trapping to play a minor role in determining QE_{ET} for the ensemble. We find a quantitative agreement between ensemble QE_{ET} and the previously reported quantum yield of H_2 generation using CdS–CaI complexes.[1] Thus the key to more efficient photochemical H_2 generation lies in improving the efficiency of ET from CdS NRs to CaI by manipulating the individual contributions of k_{ET} and k_0. Finally, the model predicts that the fraction of CdS NRs that have no CaI adsorbed limits the maximum achievable value of QE_{ET} for the ensemble. The kinetic model that accounts for heterogeneity of CdS–CaI complexes provides quantitative insights into factors that play a critical role in photochemical H_2 generation.

Details of the preparation and characterization of the CdS NRs and CaI have been described previously.[1, 2] CdS NRs used in this study had an average length of 21.5 nm and an average diameter of 4.3 nm. The CdS NR surface was functionalized with 3-mercaptopropanoic acid (3-MPA), which enabled aqueous solubility and an electrostatic interaction with CaI. CaI binds to the CdS NRs via the attraction between the negatively charged carboxylate groups of deprotonated 3-MPA and a positively charged region on the surface of the enzyme (Scheme 1).[1] This interaction is analogous to the *in vivo* binding of the electron-donating protein ferredoxin with the same positively charged region of the CaI protein surface.[1, 5] The experimental details of sample preparation are described in Section I of the ESI†.

To monitor the relaxation kinetics of photoexcited CdS NRs with and without adsorbed CaI, we used TA spectroscopy. The laser setup has been described previously,[14] and relevant experimental details are described in Section II of the ESI†. Photoexcitation of CdS NRs at 400 nm gives rise to a transient bleach feature corresponding to the band gap at 471 nm (Fig. S2, ESI†). The magnitude of the bleach is proportional to the population of electrons filling the lowest lying $1\sigma_e$ electron level of CdS NRs and is independent of the valence band hole population.[15, 16] Thus, the decay of the bleach signal for CdS NRs without CaI represents the kinetics of electrons depopulating the $1\sigma_e$ level by radiative and nonradiative recombination with the photoexcited hole and by electron trapping. We note that CaI does not have a detectable signature in the TA spectrum at the concentrations used here.

As discussed in Section IV, ESI† and shown in Fig. S3, ESI†, the TA decay curve for CdS NRs has a complicated functional form. This is commonly observed with semiconductor nanocrystals.[10, 17] We observe three time windows of distinct decay shapes in the relaxation of the CdS NR bleach feature. At short delay times, a fast (~1 ps) exponential decay component constitutes 12% of the overall decay and has recently been assigned to exciton localization.[17] Most of the decay occurs in the intermediate time regime and can be fit with a stretched exponential. At long delay times (>100 ns), with the amplitude down to 2% of the initial value, the kinetics change to a much slower decay and the stretched exponential fails to describe its shape. The origin of this long-lived component remains unknown and will not be addressed here. Although the decay of the CdS NR TA signal intensity occurs over a broad range of time, most of the change in the signal intensity upon addition of CaI occurs in the window of 1-100 ns.[2] Thus, the 1-100 ns time regime is the most relevant for understanding ET kinetics in this system and will be the focus for the remainder of this work.

To analyze the band edge bleach recovery of CdS NRs in the 1–100 ns time window, we use a kinetic model for excited state decay that explicitly includes the number distribution of electron trap sites per CdS NR in the ensemble sample. A similar model was developed for the study of quenching kinetics of luminescent probes in micellar systems,[18, 19] and has more recently been employed to study the kinetics of carrier trapping in nanocrystals,[10, 20] as well as energy,[21, 22] hole[16] and electron transfer[23] in nanocrystal–acceptor complexes. The merit of this model is that it reveals the intrinsic rate constants for electron relaxation. The decay of the TA signal can be modeled as the survival probability of the electron in the $1\sigma_e$ electron state, $P_{CdS}(t)$, because $P_{CdS}(t)$ is directly proportional to $\Delta A(t)$. This model assumes that, in this time window, trapping, recombination, and ET are not dominated by diffusion. For an ensemble of NRs, $P_{CdS}(t) = \sum_{N_{tr}=0}^{\infty} P(N_{tr}) P_{CdS}(t, N_{tr})$, where $P(N_{tr})$ is the probability that a NR has N_{tr} traps and $P_{CdS}(t, N_{tr})$ is the conditional survival probability for a NR that has N_{tr} traps. The model for $P_{CdS}(t, N_{tr})$ is the master equation:

$$\frac{dP_{CdS}(t, N_{tr})}{dt} = -(k_0 + k_{tr} N_{tr}) P_{CdS}(t, N_{tr}). \qquad (1)$$

Here k_0 is the sum of rate constants for radiative and nonradiative recombination of the electron with the hole, and k_{tr} is the rate constant for electron trapping. At low concentrations of traps, one can find $P(N_{tr})$ using equilibrium statistical mechanics for non-interacting particles. In the grand canonical ensemble, $P(N_{tr})$ is a Poisson distribution.[10, 24] After solving Eq. 1 and averaging over the Poisson distribution $P(N_{tr})$ (Section V, ESI†), $P_{CdS}(t)$ has the solution[24]

$$P_{CdS}(t) = a_{CdS} \exp\{-k_0 t + \langle N_{tr} \rangle (e^{-k_{tr} t} - 1)\}, \qquad (2)$$

where $\langle N_{tr} \rangle$ is the average number of traps in the ensemble. This model allows for the simultaneous determination of k_0, k_{tr}, and $\langle N_{tr} \rangle$. In section VI of the ESI† we derive an expression that allows for fluctuations in k_{tr} at the level of second cumulant approximation, but find that they do not lead to a statistically better fit. Thus, a single value of k_{tr} is sufficient to describe the data.

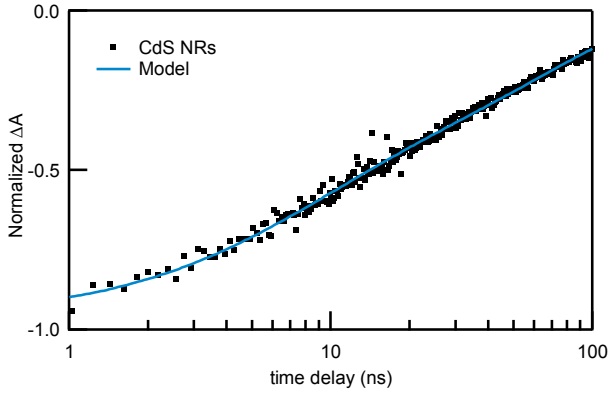

Fig. 1. TA kinetics of CdS NRs in the time window of 1–100 ns showing the fit of the kinetic model (Eq, 2) in blue.

Fig. 1 shows the TA decay of CdS NRs in the 1–100 ns time window with a fit to Eq. 2. Eq. 2 has an inherent correlation of parameters, meaning that different combinations of $\langle N_{\mathrm{tr}}\rangle$ and k_{tr}, for example, can give the same fit. We used the bootstrapping Monte Carlo method to determine the average value and corresponding 95% confidence interval for each parameter (Section VII, ESI†). The resulting fit parameters are given in Table 1. The k_0 value of 1.5×10^7 s^{-1} describes electron-hole recombination pathways and is dominated by recombination of a $1\sigma_e$ electron with a surface-trapped hole because hole trapping is very fast (ps) in CdS NRs.[25] Electron trapping is 7-fold faster than recombination, with a rate constant of 1.1×10^8 s^{-1}. The average number of traps is 0.59 in this sample, meaning that 33% of the NRs have one electron trap, and 55% have none. Because of the low electron trap density, the ensemble measurement of the excited state decay, and the associated average lifetime, is dominated by k_0. Similar trapping rates and trap densities have been previously determined for CdS NRs and CdSe QDs using the same kinetic model.[10, 24]

Table 1 Electron decay parameters for CdS NRs and CdS–CaI complexes

CaI:CdS molar ratio	k_0 (10^7 s^{-1})[a]	$\langle N_{\mathrm{tr}}\rangle$[a]	k_{tr} (10^8 s^{-1})[a]	$\langle N_{\mathrm{CaI}}\rangle$[b]	k_{ET} (10^7 s^{-1})[b]
0.00:1	1.5 ± 0.1	0.59 ± 0.04	1.1 ± 0.2	–	–
0.14:1	↓	↓	↓	0.13 ± 0.02	2.4 ± 0.6
0.59:1	↓	↓	↓	0.42 ± 0.04	↓
1.14:1	↓	↓	↓	0.68 ± 0.05	↓
1.75:1	↓	↓	↓	0.76 ± 0.06	↓

a Values found by fitting CdS NR kinetic trace (Fig. 1) with Eq. 2.
b Result of global fit of data in Fig. 2 to Eq. 3 by holding k_0, k_{tr}, and $\langle N_{\mathrm{tr}}\rangle$ fixed, defining k_{ET} as a global parameter between data sets containing CaI and allowing $\langle N_{\mathrm{CaI}}\rangle$ to vary between data sets.
Uncertainties associated with each fit parameter are 95% confidence intervals.

The presence of CaI introduces ET as an additional pathway by which photoexcited electrons in CdS NRs can decay. Fig. 2 shows the kinetic traces of CdS–CaI complexes with molar ratios of CaI:CdS in the range of 0.14:1 to 1.75:1. As the CaI:CdS molar ratio increases, the bleach feature of CdS recovers more quickly due to the increasing ET rate.[2] Mixing of CdS NRs and CaI to form complexes results in a distribution in the number of CaI adsorbed on each NR. At CaI:CdS molar ratios close to 1:1, we treat the adsorption events as independent of each other because CaI occupies a small fraction of the available surface area.[1] Thus, the number of CaI adsorbed on each CdS NR can be described by a Poisson distribution, $P(N_{\mathrm{CaI}})$. To analyze the TA decays in Fig. 2, we use a similar treatment as described above to account for the Poisson distributions of both the electron traps and adsorbed electron acceptors. This allows us to determine k_{ET} and the average number of CaI moieties adsorbed and capable of accepting an electron, $\langle N_{\mathrm{CaI}}\rangle$. Following a similar derivation as for $P_{\mathrm{CdS}}(t)$ as above (Section VIII, ESI†), the TA decay of CdS–CaI complexes, $P_{\mathrm{CdS-CaI}}(t)$, is found by averaging over both $P(N_{\mathrm{tr}})$ and $P(N_{\mathrm{CaI}})$.[24] The result is:

$$P_{\mathrm{CdS-CaI}}(t) = a_{\mathrm{CdS-CaI}}\exp\{-k_0 t + \langle N_{\mathrm{tr}}\rangle(e^{-k_{\mathrm{tr}}t}-1) + \langle N_{\mathrm{CaI}}\rangle(e^{-k_{\mathrm{ET}}t}-1)\}. \quad (3)$$

To minimize the number of adjustable parameters, the fitting of this equation to the kinetic traces of CdS–CaI complexes was performed by fixing the values of k_0, $\langle N_{\mathrm{tr}}\rangle$ and k_{tr} found from fitting CdS NRs alone to Eq. 2 (Fig. 1). This reflects the assumption that ET introduces another decay pathway without changing the intrinsic CdS parameters in Table 1. This assumption is supported by the fact that allowing variation in k_0 and k_{tr} upon addition of CaI does not statistically improve the fit. A global fit of Eq. 3 was performed such that recursive analysis converged upon the optimum value of k_{ET} that fits all four traces containing CaI in Fig. 2 simultaneously while allowing $\langle N_{\mathrm{CaI}}\rangle$ to vary.

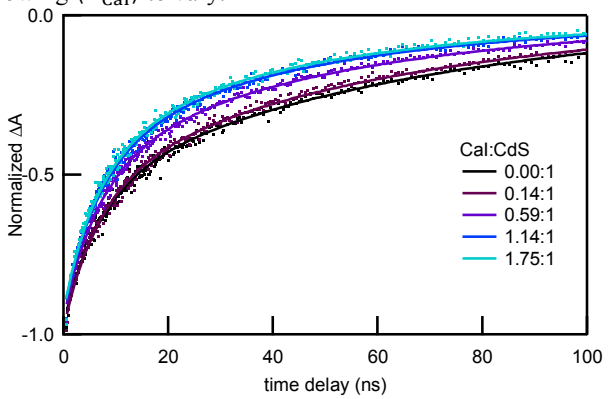

Fig. 2 TA kinetic decays of CdS–CaI complexes (points) at 470 nm for several ratios of CaI:CdS and fit functions from Eq. 3 (solid lines). The ratios listed are the mixing molar ratios during sample preparation.

The fits of Eq. 3 to the data are shown as solid lines in Fig. 2. Extracted global fit parameters for ET are given in the last two columns of Table 1. Similar values were obtained when fitting our previously published electron decay kinetics in CdS–CaI complexes using Eqs. 2 and 3 (Table S1, ESI†). Because of possible variations in the CdS NR interaction with CaI, we examined the possibility that there is a distribution in the value of k_{ET}. Using the second cumulant approximation, we included a parameter representing the variance in the values of k_{ET}. This additional parameter did not improve the fit to the data (Section VI, ESI†). This implies that, while variations in k_{ET} may exist, they do not make a measurable contribution to the TA decays reported here.

The value of k_{ET} (2.4×10^7 s^{-1}) for ET from photoexcited CdS to CaI is within an order of magnitude of k_0 and k_{tr} for CdS NRs, resulting in a direct competition between these processes. While k_0 and k_{tr} are properties of CdS NRs, k_{ET} is determined by the electron pathway, which involves electron tunneling for a considerable distance from the NR surface to the distal [FeS] cluster of the enzyme.[2] The values of $\langle N_{\mathrm{CaI}}\rangle$ in Table 1 increase with increasing CaI:CdS molar ratios and are consistently smaller than the mixing ratios. This observation may point to the presence of CaI adsorbed with orientations that prevent ET and/or to an equilibrium adsorption/desorption process that leaves some CaI free in solution.

For each individual CdS–CaI complex in the ensemble, competition between the processes described by k_0, k_{tr} and k_{ET} depends on the number of traps and enzymes adsorbed (N_{tr} and N_{CaI}). For each CdS–CaI complex, $\mathrm{QE}_{\mathrm{ET}} = k_{\mathrm{ET}}N_{\mathrm{CaI}}/(k_0 + k_{\mathrm{tr}}N_{\mathrm{tr}} + k_{\mathrm{ET}}N_{\mathrm{CaI}})$. For example, in the case of a CdS NR with zero traps and one CaI adsorbed, $\mathrm{QE}_{\mathrm{ET}} = 62\%$, while for a NR with one trap and one CaI, $\mathrm{QE}_{\mathrm{ET}} = 16\%$. Note that dividing the numerator and denominator of this expression by k_0 reveals that $\mathrm{QE}_{\mathrm{ET}}$ does not depend on the individual values of the intrinsic rates. Rather, it depends only on the ratios k_{ET}/k_0 and k_{tr}/k_0.

To understand the contribution of each electron decay process to photochemical H_2 generation in solutions of CdS–CaI complexes, it is important to examine the behavior of $\mathrm{QE}_{\mathrm{ET}}$ for the ensemble sample, which can be calculated by integrating

$P_{\mathrm{CdS}}(t)$ and $P_{\mathrm{CdS-CaI}}(t)$ (Eq. S30, Section X, ESI†). For this system, $\mathrm{QE_{ET}}$ of the ensemble depends strongly on k_{ET}/k_0 but weakly on k_{tr}/k_0, as shown in Fig. S6a (Section X of ESI†). To illustrate the behavior of ensemble $\mathrm{QE_{ET}}$, we take the example of $\langle N_{\mathrm{CaI}}\rangle = 1$ and calculate $\mathrm{QE_{ET}}$ using Eq. S30. Using the values of k_0, $\langle N_{\mathrm{tr}}\rangle$, k_{tr} and k_{ET} given in Table 1, the $\mathrm{QE_{ET}}$ would be 41%. If $\langle N_{\mathrm{tr}}\rangle = 0$, the $\mathrm{QE_{ET}}$ would only increase to 43%. The small impact that trapping has on $\mathrm{QE_{ET}}$ reflects the fact that $\langle N_{\mathrm{tr}}\rangle$ is already small. Increasing $\langle N_{\mathrm{CaI}}\rangle$ above 1 would increase $\mathrm{QE_{ET}}$, but this strategy decreases H_2 production, as we have shown previously.[1] H_2 generation requires transfer of two electrons to the same CaI moiety, and if multiple CaI are adsorbed on each NR, they compete for the second electron.[1, 2] In an ensemble, there is an upper limit on the maximum achievable value of $\mathrm{QE_{ET}}$, $\mathrm{QE_{ET}^{max}}$. For a given $\langle N_{\mathrm{CaI}}\rangle$, the fraction of NRs that do not have any CaI attached and thus do not undergo ET determines $\mathrm{QE_{ET}^{max}}$. From Poisson statistics, the fraction of NRs with one or more CaI adsorbed is $1 - e^{-\langle N_{\mathrm{CaI}}\rangle}$. The saturation value is therefore $\mathrm{QE_{ET}^{max}} = 1 - e^{-\langle N_{\mathrm{CaI}}\rangle}$. For $\langle N_{\mathrm{CaI}}\rangle = 1$, $\mathrm{QE_{ET}^{max}} = 63\%$. The ensemble value of 41% at $\langle N_{\mathrm{CaI}}\rangle = 1$ achieved with the rate constants characteristic of our current system is already ~2/3 of $\mathrm{QE_{ET}^{max}}$. A relatively modest increase in k_{ET}/k_0 by a factor of 10-100 would be sufficient to approach $\mathrm{QE_{ET}^{max}}$ (Fig. S6b, ESI†). This could be achieved through synthetic modifications of nanocrystal surface chemistry and band structure. For example, surface-capping ligands can strongly influence ET rates from a nanocrystal to an acceptor.[26] Thus k_{ET} could be increased through ligand manipulation. Alternatively, type-II nanocrystals with long-lived charge separated states could decrease k_0.[27, 28]

Finally, we compare a previously reported value of quantum yield of H_2 generation with $\mathrm{QE_{ET}}$ of a corresponding ensemble sample of CdS–CaI. In our prior work, H_2 quantum yield was 20% for a CdS–CaI solution with a CdS:CaI molar ratio of 0.67.[1] Interestingly, the value of $\mathrm{QE_{ET}}$ with the same value of CdS:CaI, obtained by interpolating between data points in Table 1, is 21%. This similarity suggests that CaI converts electrons from photoexcited CdS NRs into H_2 with close to 100% efficiency and illustrates the remarkable electrocatalytic properties of CaI.[29] It also highlights the point that the key to improving H_2 production is in increasing $\mathrm{QE_{ET}}$.

In summary, we have shown that a kinetic model that includes distributions in electron traps and adsorbed enzymes describes the kinetics of ET between CdS NRs and CaI in the time window of 1–100 ns. The model allows us to determine the intrinsic rate constants for electron-hole recombination, electron trapping, and ET. $\mathrm{QE_{ET}}$ depends strongly on the ratio of the rate constants for ET and electron-hole recombination, but only weakly on electron trapping. The maximum $\mathrm{QE_{ET}}$ saturates at a value determined by the fraction of NRs with no CaI moieties adsorbed. The current CdS–CaI system has a $\mathrm{QE_{ET}}$ value that is two-thirds of the maximum. The relatively simple model used here captures the essential kinetics of ET and provides guidance on the relevant design parameters that could be manipulated to optimize photochemical redox reactions using nanocrystal-enzyme hybrids.

CdS NR synthesis was supported by the NSF CAREER Award no. CHE-1151151 (M.B.W. and G.D.). TA measurements and kinetic modeling were supported by U.S. Department of Energy, Office of Basic Energy Sciences, Division of Materials Sciences and Engineering under Award DE-SC0010334 (J.K.U., M.B.W., G.D.). K.A.B. and P.W.K. gratefully acknowledge funding support from the U.S. Department of Energy, Office of Science, Basic Energy Sciences, Division of Chemical Sciences, Geosciences, and Biosciences; and support of the U.S. Department of Energy under Contract No. DE-AC36-08-GO28308 with the National Renewable Energy Laboratory for CaI purification, and biochemical studies.

Notes and references

[a] *Department of Chemistry and Biochemistry, University of Colorado Boulder, Boulder, Colorado 80309, United States. E-mail: gordana.dukovic@colorado.edu*
[b] *Biosciences Center, National Renewable Energy Laboratory, Golden, Colorado 80401, United States.*

† Electronic Supplementary Information (ESI) available: Experimental details, transient absorption spectra and kinetics, kinetic model derivations, rate constant fluctuations, error analysis, additional transient absorption measurements and quantum efficiency analysis. See DOI: 10.1039/c000000x/

1. K. A. Brown, M. B. Wilker, M. Boehm, G. Dukovic and P. W. King, *J. Am. Chem. Soc.*, 2012, **134**, 5627-5636.
2. M. B. Wilker, K. E. Shinopoulos, K. A. Brown, D. W. Mulder, P. W. King and G. Dukovic, *J. Am. Chem. Soc.*, 2014, **136**, 4316-4324.
3. B. L. Greene, C. A. Joseph, M. J. Maroney and R. B. Dyer, *J. Am. Chem. Soc.*, 2012, **134**, 11108-11111.
4. K. A. Brown, Q. Song, D. W. Mulder and P. W. King, *Acs Nano*, 2014, **8**, 10790-10798.
5. K. A. Brown, S. Dayal, X. Ai, G. Rumbles and P. W. King, *J. Am. Chem. Soc.*, 2010, **132**, 9672-9680.
6. C. Hamon, A. Ciaccafava, P. Infossi, R. Puppo, P. Even-Hernandez, E. Lojou and V. Marchi, *Chem. Commun.*, 2014, **50**, 4989-4992.
7. Y. S. Chaudhary, T. W. Woolerton, C. S. Allen, J. H. Warner, E. Pierce, S. W. Ragsdale and F. A. Armstrong, *Chem. Commun.*, 2012, **48**, 58-60.
8. A. Parkin, J. Seravalli, K. A. Vincent, S. W. Ragsdale and F. A. Armstrong, *J. Am. Chem. Soc.*, 2007, **129**, 10328-10329.
9. T. W. Woolerton, S. Sheard, Y. S. Chaudhary and F. A. Armstrong, *Energ. Environ. Sci.*, 2012, **5**, 7470-7490.
10. K. E. Knowles, E. A. McArthur and E. A. Weiss, *Acs Nano*, 2011, **5**, 2026-2035.
11. M. Jones and G. D. Scholes, *J. Mater. Chem.*, 2010, **20**, 3533-3538.
12. A. F. van Driel, I. S. Nikolaev, P. Vergeer, P. Lodahl, D. Vanmaekelbergh and W. L. Vos, *Phys Rev B*, 2007, **75**, 035329.
13. M. Jones, S. S. Lo and G. D. Scholes, *J. Phys. Chem. C*, 2009, **113**, 18632-18642.
14. H. W. Tseng, M. B. Wilker, N. H. Damrauer and G. Dukovic, *J. Am. Chem. Soc.*, 2013, **135**, 3383-3386.
15. V. I. Klimov, *Annu Rev Phys Chem*, 2007, **58**, 635-673.
16. J. E. Huang, Z. Q. Huang, S. Y. Jin and T. Q. Lian, *J. Phys. Chem. C*, 2008, **112**, 19734-19738.
17. K. Wu, W. Rodríguez-Córdoba and T. Lian, *J. Phys. Chem. B*, 2014, DOI: 10.1021/jp504703t.
18. P. P. Infelta, M. Gratzel and J. K. Thomas, *J. Phys. Chem.*, 1974, **78**, 190-195.
19. M. Tachiya, *Chem. Phys. Lett.*, 1975, **33**, 289-292.
20. S. Sadhu and A. Patra, *J. Phys. Chem. C*, 2011, **115**, 16867-16872.
21. G. A. Beane, A. J. Morfa, A. M. Funston and P. Mulvaney, *J. Phys. Chem. C*, 2012, **116**, 3305-3310.
22. S. Sadhu and A. Patra, *Chemphyschem*, 2013, **14**, 2641-2653.
23. A. J. Morris-Cohen, M. T. Frederick, L. C. Cass and E. A. Weiss, *J. Am. Chem. Soc.*, 2011, **133**, 10146-10154.
24. S. Sadhu, M. Tachiya and A. Patra, *J. Phys. Chem. C*, 2009, **113**, 19488-19492.
25. K. F. Wu, H. M. Zhu, Z. Liu, W. Rodriguez-Cordoba and T. Q. Lian, *J. Am. Chem. Soc.*, 2012, **134**, 10337-10340.
26. M. B. Wilker, K. J. Schnitzenbaumer and G. Dukovic, *Isr. J. Chem.*, 2012, **52**, 1002-1015.
27. S. S. Lo, T. Mirkovic, C. H. Chuang, C. Burda and G. D. Scholes, *Adv Mater*, 2011, **23**, 180-197.
28. H. M. Zhu and T. Q. Lian, *Energ Environ Sci*, 2012, **5**, 9406-9418.

29. K. A. Vincent, A. Parkin and F. A. Armstrong, *Chem Rev*, 2007, **107**, 4366-4413.